JOURNAL OF MATERIALS SCIENCE 33 (1998) 4321–4325

Sintering and microstructure development in the system $MgO–TiO_2$

Y. B. LEE, H. C. PARK, K. D. OH
Department of Inorganic Materials Engineering, Pusan National University, Pusan 609-735, Korea

F. L. RILEY
Department of Materials, University of Leeds, Leeds, LS2 9JT, UK

The sintering and microstructure development of magnesia containing 0–10 wt % TiO_2 at temperatures in the range 1300–1600 °C have been investigated. The addition of TiO_2 markedly promoted densification at relatively low temperature, and grain growth. Excess TiO_2 over the solid solubility limit of TiO_2 (0.3 wt %) reacted with magnesia to form inter- and intra-granular magnesium titanate (Mg_2TiO_4) above 1300 °C. The grain size of MgO increased with increasing TiO_2 content, and densification was mainly governed by MgO grain growth.

1. Introduction

Magnesium oxide (MgO), because of its high melting point (approximately 2800 °C), chemical stability in a basic environment and high electric resistivity, is widely used as an industrial refractory and a high temperature insulator [1, 2]. However, it has poor thermal shock resistance because of its high (approximately 13 MK^{-1}) thermal expansion coefficient [3]. Industrial trends to more severe environments for more efficient operations to yield high-quality products, mean that magnesia may have wider application, if its strength and thermal shock characteristics can be improved.

Doping may introduce lattice defects or alter grain boundary characteristics, which affect second-phase particle mobility, M_p, and grain boundary mobility, M_b [4]. A large M_p/M_b ratio will produce a fine-grained microstructure with intergranular second-phase particles, because the second-phase particles remain at the boundary and exert a pinning effect. A small M_p/M_b ratio may result in a large-grained microstructure with intragranular second-phase particles, because the grain boundary breaks away from the second-phase particles, and the pinning effect is lost. It is reported [5, 6] that the addition of TiO_2 up to the solubility limit promotes the grain growth of α-Al_2O_3 in the TiO_2–Al_2O_3 system. However, beyond the TiO_2 solubility limit, second-phase Al_2TiO_5 retards grain growth, by exerting a pinning effect on the grain boundaries.

A number of papers report on the role of additives in the sintering of MgO [7–9]. Additions of tetravalent Si, Ti and Zr enhance sintering. The $MgO–TiO_2$ binary phase diagram shows that an $MgO–TiO_2$ solid solution decomposes eutectoidally on cooling into Mg_2TiO_4 and MgO at 1756 °C [10]. This suggests the possibility of strengthening MgO materials with particulate Mg_2TiO_4 dispersions. No work has been reported on the sintering and microstructure development of magnesia strengthened with a dispersed second phase.

This study was undertaken to investigate the effect of addition of TiO_2 on the sintering behaviour of MgO.

2. Experimental procedure

Reagent grade magnesium sulphate ($MgSO_4 \cdot 7H_2O$) and titanyl sulphate ($TiOSO_4 \cdot 2H_2O$) were used in this investigation. The amount of addition was 0.5, 1, 2, 4, 6, 8 and 10 wt %, calculated as TiO_2. The salts were dissolved in distilled water, and the mixed solution was freeze dried at −50 °C and 0.6 Pa. The dry powder was calcined in air at 1200 °C for 2 h. Calcination was followed by the results of thermogravimetric and differential thermal analysis. Discs 12 mm diameter by 50 mm were die-pressed at 15 MPa, followed by isostatically pressing at 150 MPa and sintered in air in an electric furnace at 1400–1600 °C for 2 h with a heating rate of 4 °C min^{-1}. After sintering, samples were rapidly cooled in air to room temperature.

Phase analyses and the MgO lattice parameter were obtained from X-ray diffraction (XRD) patterns. Sintering shrinkage was determined by a computer-controlled high temperature dilatometer, using a heating rate of 4 °C min^{-1}. Specific surface area and the particle size distribution of calcined powders, were determined by the nitrogen adsorption Brunaver–Emmett–Teller (BET) method, and X-ray sedimentation method. Bulk densities of sintered samples were measured using Archimedes' principle. For microstructural evaluation, sintered samples were polished with SiC abrasive papers, finished with 0.5 μm Al_2O_3 powder on a velvet cloth, and thermally etched.

TABLE I Characteristics of MgO powder after calcination at 1200 °C for 2 h

Powder	Specific surface area ($m^2 g^{-1}$)	Particle size (μm)	Chemical component (wt %)[a]					
			MgO	CaO	Na_2O	K_2O	Fe_2O_3	TiO_2
MgO	6.80	<1.5	99.54	0.26	0.19	0.01	–	0.02

[a] XRF analysis.

Fracture surfaces were gold coated and examined by scanning electron microscopy (SEM).

3. Results and discussion

The characteristics of calcined MgO powder are summarized in Table I; powder generally consisted of spherical particles of size <1.5 μm.

MgO–2 wt % TiO_2 samples sintered at 1300–1600 °C were examined by XRD (Fig. 1). Integrated relative intensity ratios for MgO, Mg_2TiO_4 and TiO_2 (rutile) are shown in Fig. 2. With increasing temperature, the diffraction peak of TiO_2 decreased in intensity, and disappeared at 1500 °C. Mg_2TiO_4 was detected at approximately 1300 °C, increased to 1400 °C, and then remained constant.

It is expected that solution of TiO_2 in MgO slightly changes the MgO lattice parameter because the ion radii of Ti^{3+} and Ti^{4+} are significantly different from Mg^{2+} (78 pm). To examine the change of the MgO lattice parameter after firing at 1600 °C, XRD analyses were carried out using a step scanning method on sintered surfaces, using quartz as an internal standard material. The deviations from the lattice constant of pure MgO are shown in Fig. 3. The negative deviation was almost constant at about 0.1%, and independent of TiO_2 amount in the range 2–10 wt %. It is postulated that the solution of TiO_2 leads to constriction of the MgO lattice, due to the residual stress formed during cooling.

Fig. 4 shows the ratio of the integrated relative intensities of the TiO_2 (1 1 0) and MgO (2 0 0) peaks after firing the 0.5, 1 and 2 wt % TiO_2 mixtures at 1300 °C for 2 h. Extrapolation using least squares leads to an intercept at approximately 0.3 wt %: therefore, the solid solubility of TiO_2 in MgO is estimated

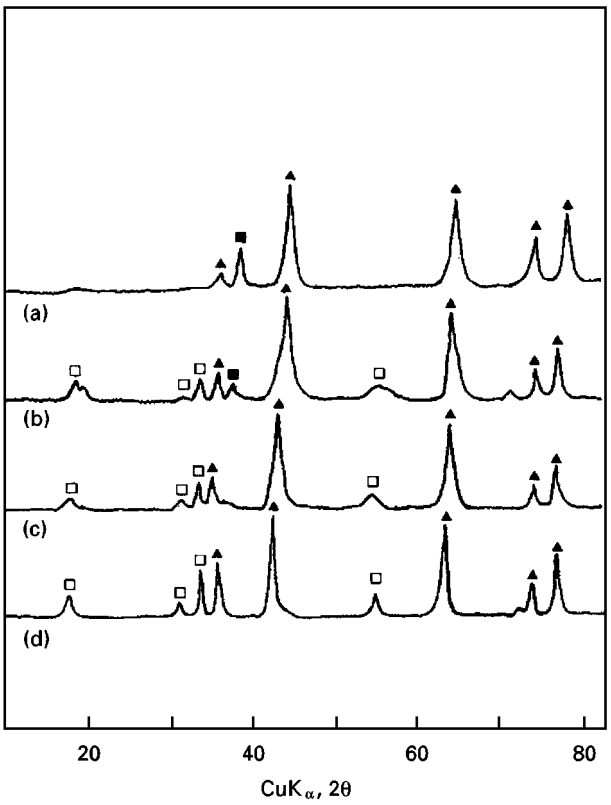

Figure 1 X-ray diffraction patterns of 2 wt % TiO_2–MgO sintered at (a) 1300, (b) 1400, (c) 1500 and (d) 1600 °C for 2 h. ■ TiO_2, □ Mg_2TiO_4, ▲ MgO.

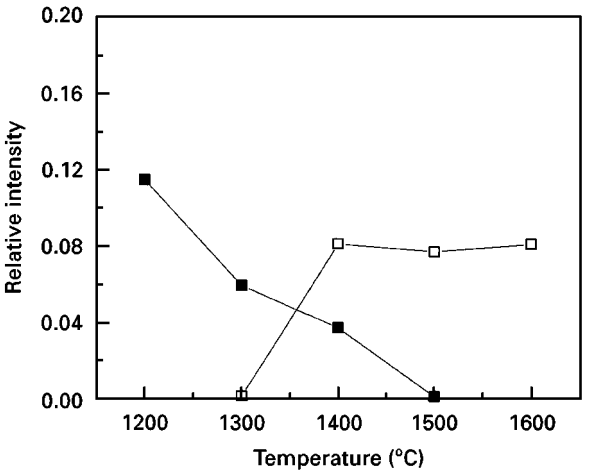

Figure 2 Integrated relative intensity ratios of TiO_2 and Mg_2TiO_4 versus MgO in 2 wt% TiO_2–MgO. ■ TiO_2/MgO, □ Mg_2TiO_4/MgO.

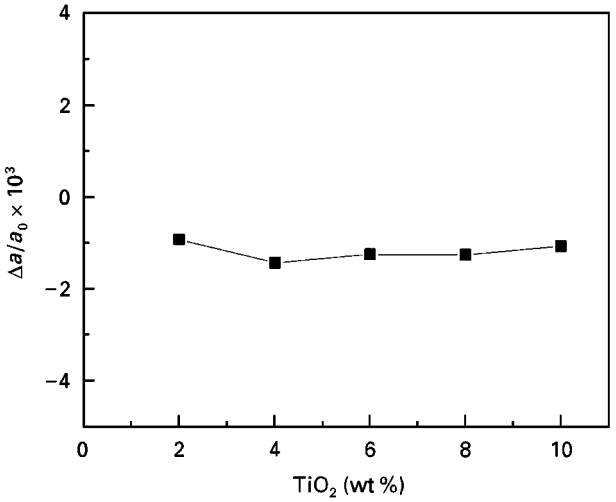

Figure 3 Deviations from lattice constant, $\Delta a/a_0$, of pure MgO according to additions of TiO_2 after sintering at 1600 °C for 2 h.

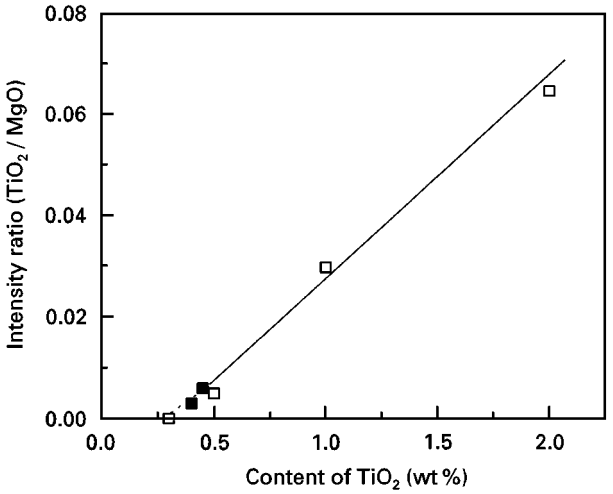

Figure 4 Ratios of integrated relative intensity of TiO_2 (1 1 0) and MgO (2 0 0) peaks (□) according to additions of TiO_2 after firing at 1300 °C for 2 h; (■) intensity ratios in 0.1 and 0.2 wt% TiO_2–MgO.

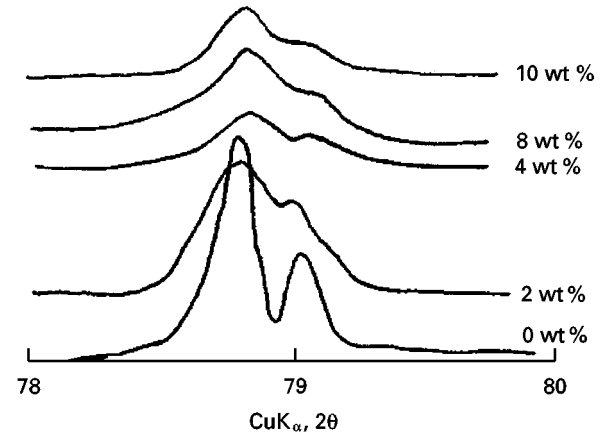

Figure 5 X-ray diffraction profiles of MgO (2 2 2) peak in the specimens containing various amounts of TiO_2 after sintering at 1600 °C for 2 h.

to be ≤ 0.3 wt %. To confirm instrument sensitivity, relative intensity ratios of TiO_2 and MgO were replotted as a black square in Fig. 4, for the calcined pure MgO powder mixed with 0.1 and 0.2 wt % TiO_2 (extra grade, Junsei Chemical, Japan). Because the points correspond well with the least squares straight line for the 0.5, 1 and 2 wt % TiO_2 mixtures, it is considered that the instrument has a sensitivity to detect 0.3 wt % TiO_2. Because the evaporation of TiO_2 at 1600 °C is negligible, the intercept at 0.3 wt % TiO_2 is considered to be the solid solubility limit of TiO_2 in MgO over this temperature range, assuming no precipitation on cooling.

XRDs of MgO (2 2 2) peaks for different TiO_2 contents sintered at 1600 °C for 2 h, are shown in Fig. 5. The (2 2 2) peak in pure MgO was at 78.7° (2θ); this shifted to a lower angle and broadened, with increasing TiO_2. This is likely to be the result of a combination of TiO_2 solid solubility and lattice deformation (Fig. 3), which occurred due to the difference in thermal expansion between MgO and Mg_2TiO_4 on cooling. Also, it is considered that the degree of MgO lattice distortion will be increased proportional to the

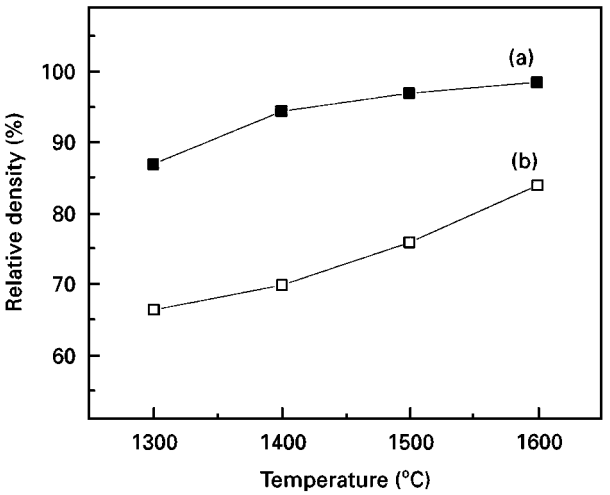

Figure 6 Relative sintered densities of (a) 0 and (b) 2 wt % TiO_2–MgO.

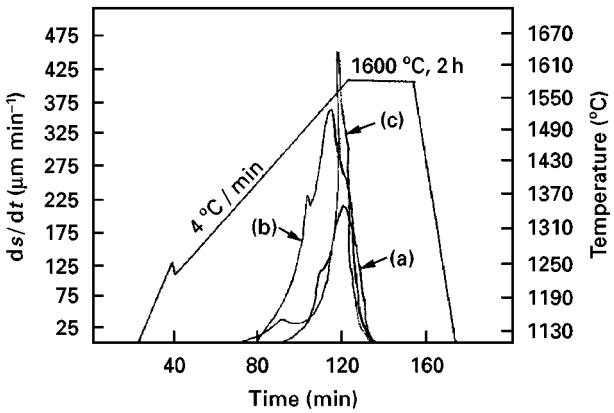

Figure 7 Nonisothermal shrinkage rate curves, ds/dt, of (a) 0, (b) 2 and (c) 4 wt % TiO_2–MgO.

amount of Mg_2TiO_4 formation, increasing with TiO_2 addition.

The relative sintered densities of 0 and 2 wt % TiO_2–MgO are shown in Fig. 6. The relative density is based on a theoretical density of 3.58 g cm^{-3} for MgO. Sintered density increased with increasing temperature. Although there are differences according to starting materials, grain growth of magnesia generally starts at 1500 °C, and then its rate increases rapidly by the dead burned effect at < 1500 °C [12]. The density of the 2 wt % TiO_2–MgO is higher (approximately 20%) than that of the 0 wt % TiO_2–MgO at all temperatures. At 1500 °C, 76% density is achieved by the 0 wt % TiO_2–MgO, and 98% by the 2 wt % TiO_2–MgO. As shown in Fig. 7, the maximum shrinkage rates were 1600, 1530 and 1580 °C, for 0, 2 and 4 wt % TiO_2. The additions of TiO_2 apparently promoted the shrinkage rate of MgO on firing. Therefore, TiO_2 promotes grain growth in MgO, and then the dead burned effect appears at relatively low temperature. On the other hand, the enhancement of densification of MgO by TiO_2 can be rationalized on the basis of cation vacancy formation [13–15]

$$TiO_2 \xrightarrow{MgO} Ti_{Mg}^{oo} + V_{Mg}'' + 2O_O^X \quad (1)$$

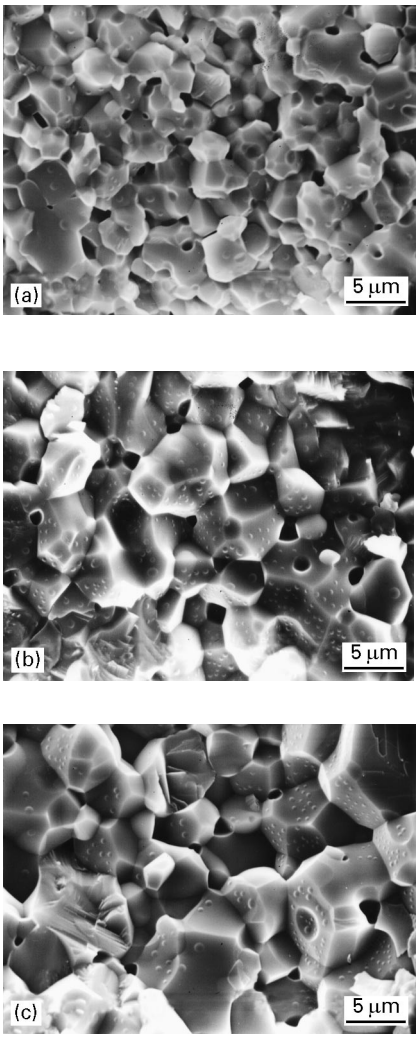

Figure 8 Scanning electron photographs of fracture surfaces of 2 wt % TiO_2–MgO sintered at (a) 1400, (b) 1500 and (c) 1600 °C for 2 h.

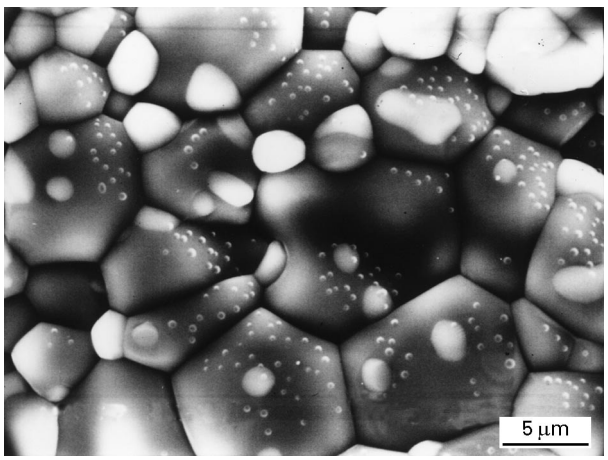

Figure 9 Scanning electron photograph of polished surface of 4 wt % TiO_2–MgO sintered at 1600 °C for 2 h.

The enhanced densification may be explained as

1. The TiO_2 dissolves in the MgO below the solid solubility limit and increases the cation vacancy concentration.

2. Above the solid solubility limit, an excess TiO_2 forms Mg_2TiO_4 compound and then increases MgO grain growth.

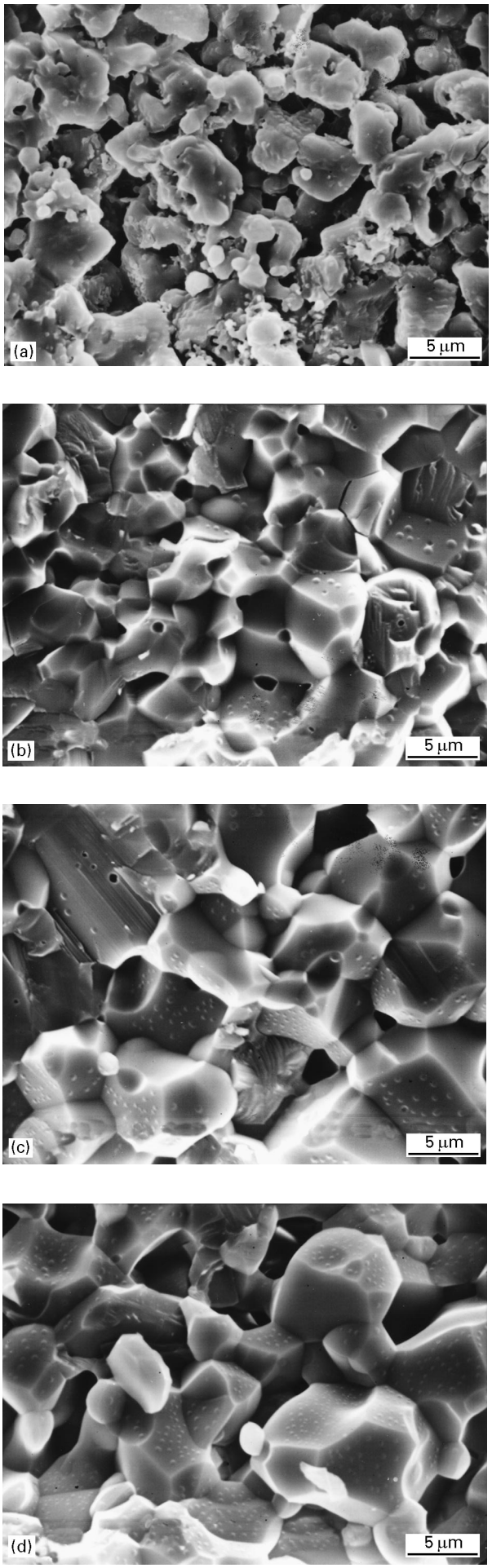

Figure 10 Scanning electron photographs of fracture surfaces of (a) 0, (b) 2, (c) 4 and (d) 10 wt % TiO_2–MgO sintered at 1600 °C for 2 h.

The sintered fracture surfaces for 2 wt % TiO_2–MgO after firing at 1400, 1500 and 1600 °C for 2 h are shown in Fig. 8. The MgO grains and intergranular pores in material sintered at 1500 and 1600 °C were relatively large compared with 1400 °C. Mg_2TiO_4 particles (shown as "white") precipitated within the grain and at the grain boundary of 10 μm MgO grains ("black"; Fig. 9).

Microstructures of the fracture surface of the 0, 2, 4 and 10 wt % TiO_2–MgO sintered at 1600 °C are shown in Fig. 10. The grain size of MgO increased and a few large intergranular pores existed, with increasing TiO_2 content. The increase in grain size was not fully understood, and was not investigated further in the present study. However, it was obvious that there was no strong pinning effect at higher volume fractions of the second phase. It was assumed that grain boundary mobility had been significantly enhanced by the addition of TiO_2. From the above data, large fast growth and intragranular Mg_2TiO_4 can be qualitatively understood on the basis of the doping effect on M_b alone.

As MgO is mainly ionic, the properties related to defects are controlled by the concentration and the nature of the dopant, Ti^{4+}. The solid solubility limit of the dopant is less than 0.3 wt % in MgO (Fig. 4). Within solid solubility limit, Ti^{+4} has the active role of forming defects that promote diffusion. According to Schottky equilibrium, Equation 1 results in an increase in cation and vacancy concentrations. Therefore, the sintering of MgO is accelerated by TiO_2 up to the solid solubility limit. On the other hand, above the solid solubility limit excess TiO_2 precipitates at grain boundaries and the forms Mg_2TiO_4, and Ti^{4+} (64 pm) is expected to have a smaller diffusion coefficient than that of Mg^{+2} due to its higher electric charge in spite of comparable ionic radius.

Therefore, it is considered that when Mg_2TiO_4 is formed by cation interdiffusion between MgO and TiO_2, mass transport to TiO_2 may proceed more rapidly than vice versa and then more vacancies are left on the MgO-side. As a result, grain growth of MgO is promoted with increasing TiO_2 content (Fig. 10), and the partial Mg_2TiO_4 particles exist as intragranular MgO (Fig. 9) due to the more rapid mobility of the MgO grain boundary than that of the Mg_2TiO_4 grain boundary.

4. Conclusions

An excess of TiO_2 over the solid solubility limit reacts with MgO to form Mg_2TiO_4 at higher temperatures than 1300 °C. Deviation of the lattice parameter of the MgO crystal was estimated to be under (−) 0.1% due to the addition of TiO_2. The addition of TiO_2 markedly promoted the densification of MgO at comparatively low temperatures; a density of approximately 98% of theoretical was obtained at 1200 °C in 2 h. The enhancement of densification resulted from grain growth of MgO, and the effect of Mg_2TiO_4 as a second phase to depress grain growth was not seen.

References

1. P. BUDNIKOV and S. ISKAREVICH, *Trans. Brit. Ceram. Soc.* **33** (1934) 368.
2. J. H. CHESTERS and T. R. LYNAM, *J. Amer. Ceram. Soc.* **22** (1939) 97.
3. H. EBERT and C. TINGWALDT, *Physik. Z.* **37** (1936) 471.
4. L. A. XUE, K. MEYER and I. CHEN, *J. Amer. Ceram. Soc.* **75** (1992) 822.
5. K. HAMANO, C. HWANG, Z. NAKAGAWA and Y. OHYA, *J. Ceram. Soc. Jpn* **94** (1986) 505.
6. K. A. BERRY and M. P. HARMER, *J. Amer. Ceram. Soc.* **69** (1986) 143.
7. S. KIMURA, E. YASUDA and H. KIM, *Tokyo Inst. Tech. Bull.* **117** (1973) 87.
8. A. NISHIDA, S. FUKUDA, Y. KOHTOKU and K. TERAI, *J. Ceram. Soc. Jpn* **100** (1992) 191.
9. T. C. YUAN, G. V. SRINIVASAN, J. F. JUE and A. V. VIRKAR, *J. Mater. Sci.* **24** (1989) 3855.
10. E. M. LEVIN, C. R. ROBBINS and H. F. McMURDIE, in "Phase Diagram for Ceramist" Vol. 1, edited by the ACS (The American Ceramic Society, Inc., 1969) p. 112.
11. Y. KOUICHI, T. YASUHIKO, K. YUKIHIRO, M. YOHOTARO and K. SHIUSHICHI, *J. Ceram. Soc. Jpn* **100** (1992) 797.
12. S. MATSUDA, *Taikabutsu* **45** (1993) 546.
13. J. W. NELSON and I. B. CULTER, *J. Amer. Ceram. Soc.* **41** (1958) 406.
14. G. K. LAYDEN and M. C. McQUARRIE, *ibid.* **42** (1959) 89.
15. E. A. COLBOURN and W. C. MACKROAD, *J. Mater. Sci.* **17** (1982) 3021.

Received 16 March
and accepted 18 June 1998